

Template for preparing your research report submission to PNAS using Overleaf

Author One^{a,c,1}, Author Two^{b,1,2}, and Author Three^a

^aAffiliation One; ^bAffiliation Two; ^cAffiliation Three

This manuscript was compiled on August 16, 2017

We present a conceptual and computational framework to unify today's theories of neuromuscular control called feasibility theory. We begin by describing how the musculoskeletal anatomy of the limb, the need to control individual tendons, and the physics of a motor task uniquely specify the family of all valid muscle activations that accomplish it (its 'feasible activation space'). For our example of static force production with a finger with seven muscles, computational geometry characterizes, in a complete way, the structure of feasible activation spaces as 3-dimensional polytopes embedded in 7-D. The feasible activation space for a given task is the landscape where all neuromuscular learning, control, and performance must occur. This approach unifies current theories of neuromuscular control because the structure of feasible activation spaces can be separately approximated as either low-dimensional basis functions (synergies), high-dimensional joint probability distributions (Bayesian priors), or fitness landscapes (to optimize cost functions).

Neuromechanics | Motor Control | Tendon actuation | ...

This PNAS journal template is provided to help you write your work in the correct journal format. Instructions for use are provided below.

Note: Please start your introduction without including the word "Introduction" as a section heading (except for math articles in the Physical Sciences section); this heading is implied in the first paragraphs.

Introduction

How the nervous system selects specific levels of muscle activations (i.e. a muscle activation pattern) for a given motor task continues to be hotly debated. Some suggest the nervous system either combines low-dimensional synergies (1–7), learns probabilistic representations of valid muscle activation patterns (8–11), or optimizes physiologically-tenable cost functions (12–17). At the core of this problem lies the nature of 'feasible activation spaces,' and the computational challenge of describing and understanding their high-dimensional structure (for an overview, see (18)). A feasible activation space is the family of valid solutions (i.e. muscle activation patterns) available to the nervous system to produce a given motor task. Fig. 1 illustrates the neuromechanical interactions that define the feasible activation space for a particular task.

The most the nervous system can do, therefore, is select a specific muscle activation pattern from within the feasible activation space—as muscle activation patterns outside of this space are, by definition, inappropriate for the task. In fact, the feasible activation space defines the landscape upon which all neuromuscular learning and performance must occur. Understanding neuromuscular control is, therefore, equivalent to understanding how the nervous system finds, explores, inhabits, and exploits the structure of feasible acti-

vation spaces (1–6, 22).

But the 'curse of dimensionality' (23–25) makes it computationally challenging to calculate, describe, and understand the nature and structure of high-dimensional feasible activation spaces (4, 12, 19, 20, 26–28)—even for an isolated human finger or cat leg generating everyday static forces (1, 18, 29, 30). This is due to the computational complexity of algorithms applied upon high dimensional spaces.

Current theories of neuromuscular control are alternative responses to the curse of dimensionality, which at times can be seen as competing, rather than complementary. However, the fundamental neuromechanics of the limb and the physics of the task are the common ground for all theories. Thus, understanding the nature and structure of feasible activation spaces would help compare, contrast and combine these alternative approaches to neuromuscular control.

We now propose a conceptual and computational framework to provide complete characterizations of feasible activation spaces, thereby contextualizing and unifying multiple theories of neuromuscular control. As an example, we leverage prior work (1, 21, 31) to now describe the structure of the feasible activation space for the seven muscles of the index finger when producing static fingertip force. This is the type of fingertip force observed when, for example, pressing hard on a table without finger movement, and is also referred to as an isometric force task. In this case, the feasible activation space is a polytope embedded in 7-dimensional muscle activation space. A polytope is the name given to bounded convex polyhedra in dimensions higher than 3. Our computational approach hinges on the efficient sampling and complete representation of the structure of high-dimensional polytopes. This then characterizes all valid muscle activation patterns. These computational

Significance Statement

Wings take flight, eyes refract light, and muscles manipulate bones within the interplaying constraints of Newtonian physics. Here we apply the basic tenets of physics to the field of neuromechanical control, to elucidate the neuro-physical-motor landscape upon which evolution and learning operate. With three interweaving hypotheses of motor control in the literature, we fill the gap between the disparate approaches by recontextualizing the problem of force control as a physical constraints problem, thereby lighting the stage of optimal, synergistic, and bayesian control.

Please provide details of author contributions here.

Please declare any conflict of interest here.

¹A.O.(Author One) and A.T. (Author Two) contributed equally to this work (remove if not applicable).

²To whom correspondence should be addressed. E-mail: author.two@email.com

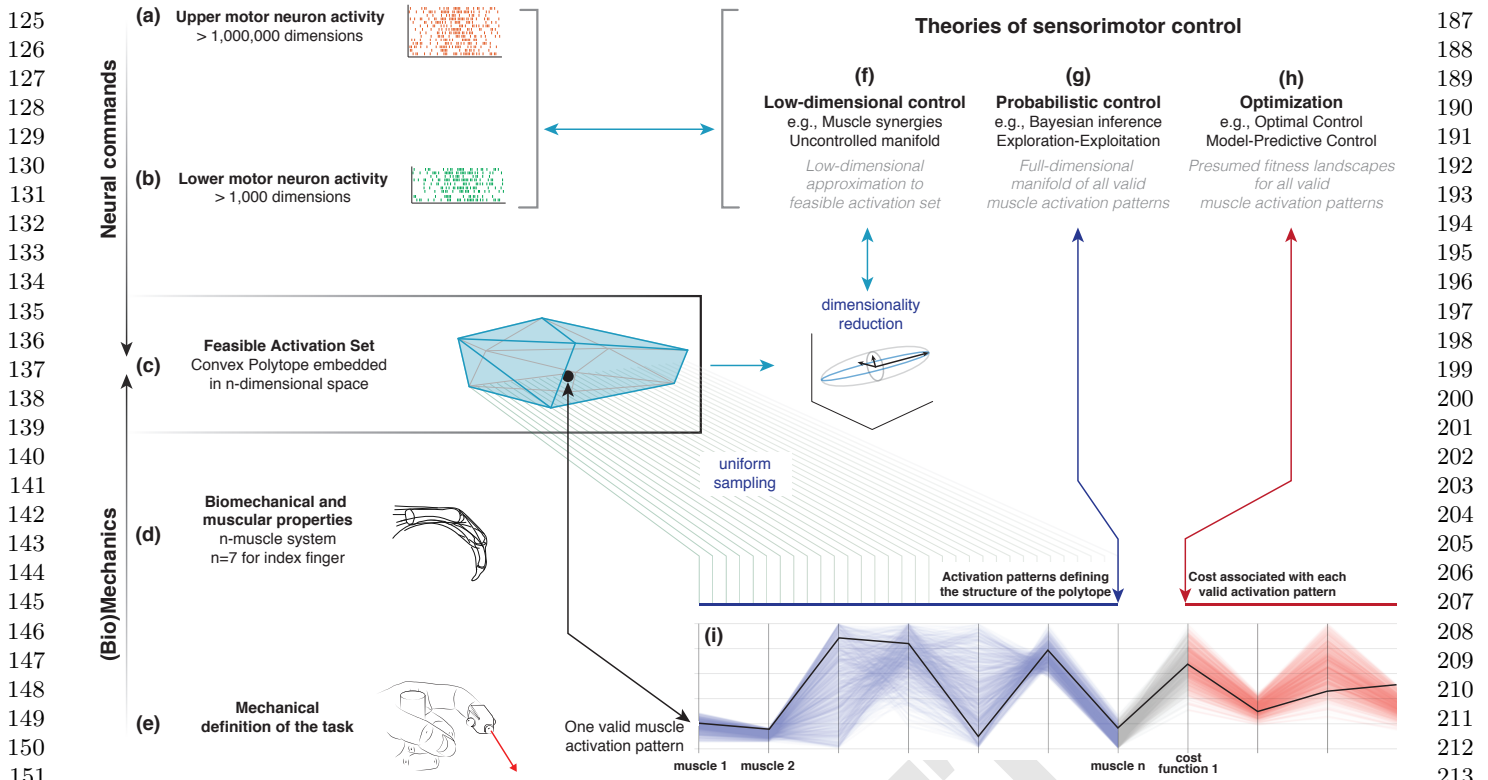


Fig. 1. Feasible activation spaces guiding sensorimotor control of a task. The descending motor command for a given task is issued by the primary motor cortex (a), which projects onto alpha-motor neuron pools in the spinal cord (b). The combined drive to all alpha-motor neurons of a muscle can be considered its total muscle activation level (a value between 0 and 1). If we consider that motor commands are sent to multiple independently controlled muscles, then the overall motor command can be conceptualized as a multi-dimensional muscle activation pattern (i.e., a point) in a high-dimensional muscle activation space (12, 19–21) (c). For that muscle activation pattern to be valid, it has to elicit muscle forces (d) capable of satisfying the mechanical requirements of the task—in this case a well directed fingertip force (e). Given the large number of muscles in vertebrates, there is muscle redundancy; there is a large number of valid muscle activation patterns that can produce a given task. We propose that our novel ability to characterize the high-dimensional structure of feasible activation spaces (i) allows us to compare, contrast and reconcile today's three dominant approaches to redundancy in sensorimotor control (f, g, h).

techniques can scale up to ~40 dimensions, which suffices to analyze the neural control of all muscles in extant vertebrate limb systems. By providing a complete characterization of all muscle activation patterns for a given motor task, we are able to compare, contrast, combine—and reconcile—today's three dominant approaches to neuromuscular control.

Results

The goal of this work is to use different perspectives to describe the high-dimensional structure of these feasible activation spaces; we then show how these spaces allow us to unify today's theories of neuromuscular control. We used our realistic index finger model to calculate the feasible activation space for the task of producing static fingertip force in the distal direction (see Fig. 1). The model represents each muscle's contribution to fingertip force as a directed force vector at the fingertip; there are 7 of these force vectors at the index fingertip. As described briefly in the Methods, Hit-and-Run is a method in polytope sampling that we use to sample from the infinite number of muscle activations within the feasible activation space. In effect, given a fingertip task force and the maximum linear fingertip forces each muscle creates, we can collect the muscle activations required to produce that task. As we can now collect thousands of muscle activation patterns for any isometric force task, we examined how the feasible activation

spaces (and their representations) change with increasing task intensity in the distal direction (Fig. 1e).

We collected points for multiple task intensities between 0% (i.e., pure co-contraction without output force) and 100% of maximal static force.

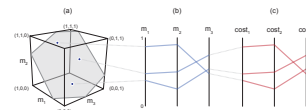
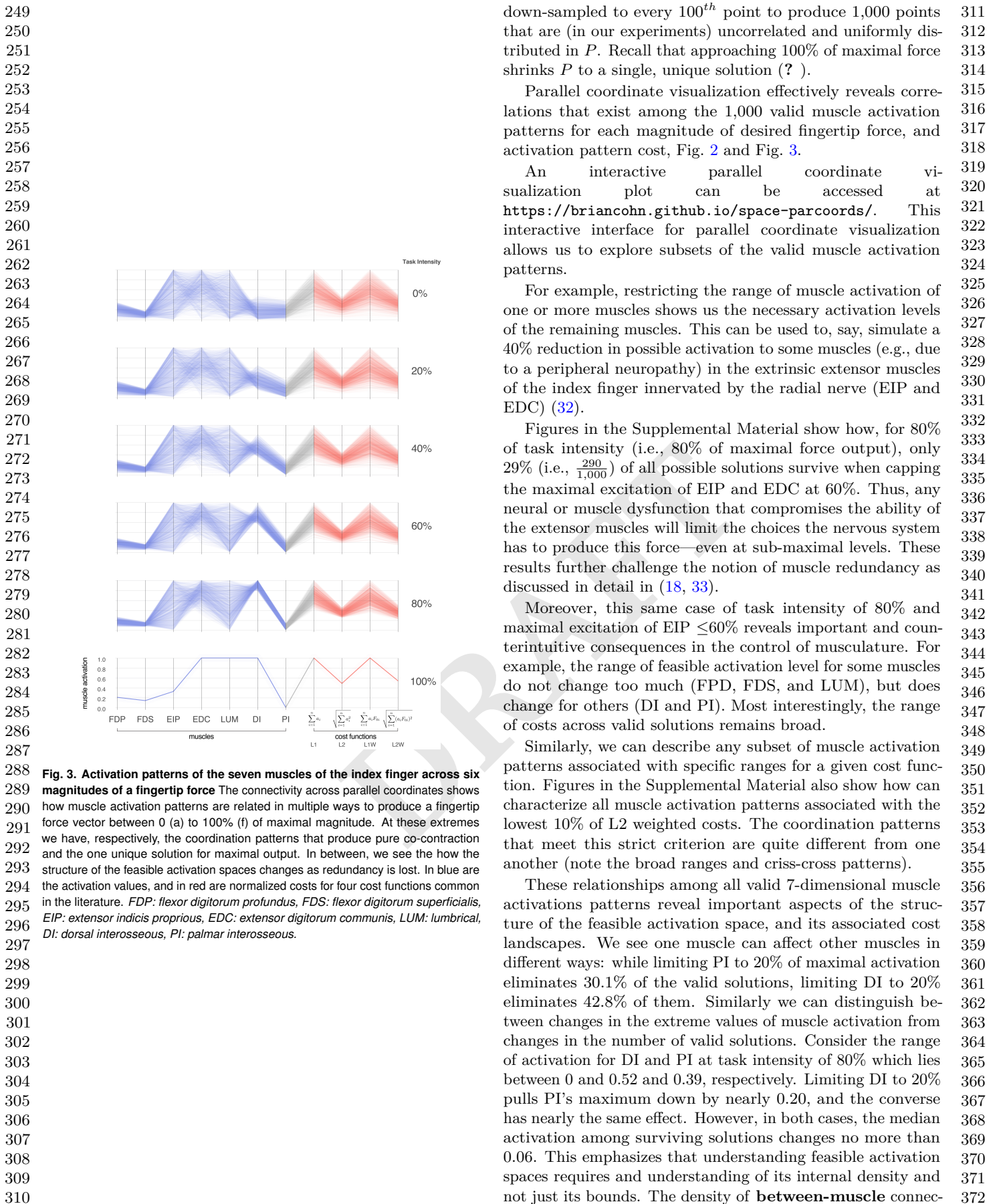


Fig. 2. Characterizing the high-dimensional structure of a feasible activation space via parallel coordinates. Consider three points (i.e., muscle activation patterns in Supplemental Fig. ??e) from the feasible activation space (a). The activation level for each muscle (i.e., the coordinates of each point) are sewn across three vertical parallel axes (b). As is common when evaluating multiple valid coordination patterns, each point can be assigned a cost as per an assumed cost function. The associated cost for each muscle activation pattern can also be shown as an additional dimension. We show three representative cost functions (c). Activation levels are bound between 0 and 1, and costs are normalized to their respective observed ranges.

Parallel coordinate visualization naturally reveals the structure of the feasible activation space. We used Hit-and-Run to sample from feasible activation spaces for 6 task intensities, labeled as task intensities α of 0.0, 0.2, 0.4, 0.6, 0.8 and 1.0. For each task intensity, we ran 100,000 Hit-and-Run iterations and



373 tivity is seen directly by the density of the lines connecting
 374 the different muscles and cost functions. The **within-muscle**
 375 density can be computed by binning points at each activation
 376 level value. 435
 436
 437
 438
 439
 440
 441
 442
 443
 444
 445
 446
 447
 448

377 Lastly, those same connecting lines in the parallel coordinate
 378 visualization allow us to characterize the interrelatedness
 379 of valid solutions in 7-dimensional space. For example, the
 380 lines connecting FDP and FDS are mostly parallel, indicating
 381 a strong positive correlation. In fact, looking at these lines
 382 allows one to directly see and understand the Pearson product-
 383 moment correlation coefficients of 0.99, -0.50, and -0.06 in the
 384 adjacent muscle pairs FDP—FDS, LUM—DI, and EIP—EDC,
 385 respectively. The interactive parallel coordinate visualization
 386 also allows for any pairwise comparison by simply dragging
 387 and reordering the vertical axes—and hovering over individual
 388 data rows highlight an individual valid activation pattern atop
 389 all others. 449
 450
 451
 452
 453
 454
 455
 456
 457
 458
 459

390 **Low-dimensional approximations to the feasible activation
 391 space.** We applied PCA (Principal Component Analysis) to
 392 the valid muscle activation patterns sampled uniformly at
 393 random from the feasible activation space. We show results for
 394 10 levels of task intensity. However, we did this in an iterative
 395 fashion to replicate the fact that experimental studies can only
 396 collect a finite amount of data from each subjects. Thus, from
 397 the total pool of 10,000 sub-sampled points sampled by Hit-
 398 and-Run (i.e., accepting every 100th point from 100,000 total
 399 samples to remove potential autocorrelation among points);
 400 sample sizes of 10, 100, and 1,000 points (i.e., simulated ‘ex-
 401 perimental’ sample sizes) were replicated 100 times each. We
 402 applied PCA to each set of sampled points. 460
 461
 462
 463
 464
 465
 466
 467
 468
 469
 470
 471
 472
 473
 474
 475
 476
 477
 478
 479
 480
 481
 482
 483
 484
 485
 486
 487

403 The variance explained by PC1 and PC2 (and its boxplot
 404 distribution) for all iterations are shown to change with task
 405 intensity for all sample sizes (Fig. 5). Explaining about 13–15%
 406 of the variance, PC3 is exactly equal to the remaining variance
 407 not explained by the first two components—this is a result of
 408 the feasible activation space being a 3-dimensional polytope
 409 P by construction (i.e., recall that 4 task constraints applied
 410 to 7 muscles produce a 3-dimensional polytope embedded in
 411 the 7-dimensional muscle activation space). 470
 471
 472
 473
 474
 475
 476
 477
 478
 479
 480
 481
 482
 483
 484
 485
 486
 487

413 The boxplots in Fig. 5 quantify how different amounts of
 414 data change the estimates of variance explained by PC1 and
 415 PC2 with task intensity (c.f. labels a vs. b vs. c). We see
 416 this dispersion is small in the center and right columns. Note
 417 that the ratio of variance explained between PC1 and PC2
 418 between 50 to 80% of task intensity is indicative of changes in
 419 the aspect ratio of the feasible activation space—which we see
 420 changes with task intensity. 488
 489
 490
 491
 492
 493
 494
 495
 496

421 Importantly, using experimentally realistic samples sizes of
 422 10 repetitions per subject (leftmost column) not only does not
 423 capture this change, but its standard deviation is large enough
 424 to blur the statistically significant differences that are known
 425 to appear with larger (but experimentally unrealistic) sample
 426 sizes. The impact of impoverishing the number of samples fed
 427 to PCA reminds us that inadequate amounts of data obfuscate
 428 the underlying changes in the structure of the data analyzed
 429 (Fig. 5). 489
 490
 491
 492
 493
 494
 495
 496

430 There were also important changes in the loadings of the
 431 PC1 and PC2 vectors. While the ratio of variance explained
 432 between PC1 and PC2 gives a sense of the aspect ratio of
 433 the feasible activation space, the loadings of PC1 and PC2
 434 speak to its orientation. Fig. 6 shows how the loadings of
 435
 436
 437
 438
 439
 440
 441
 442
 443
 444
 445
 446
 447
 448
 449
 450
 451
 452
 453
 454
 455
 456
 457
 458
 459
 460
 461
 462
 463
 464
 465
 466
 467
 468
 469
 470
 471
 472
 473
 474
 475
 476
 477
 478
 479
 480
 481
 482
 483
 484
 485
 486
 487

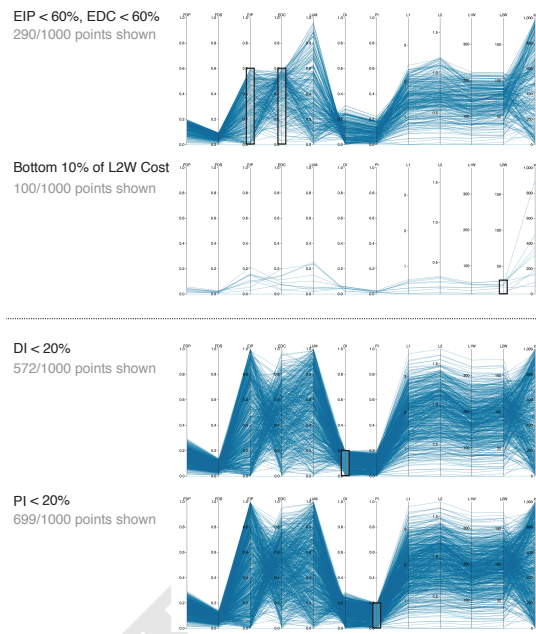


Fig. 4. Supplemental Figure: Posthoc constraints on a task intensity of 80%
 Here we show four unique examples of constraints applied to the points collected from the feasible activation space. With this, we can rapidly predict how index finger control must change in the event of weakness in specific muscles. We also can see how many points remain once the constraints are added—signaling how the structure of the feasible force space is affected.

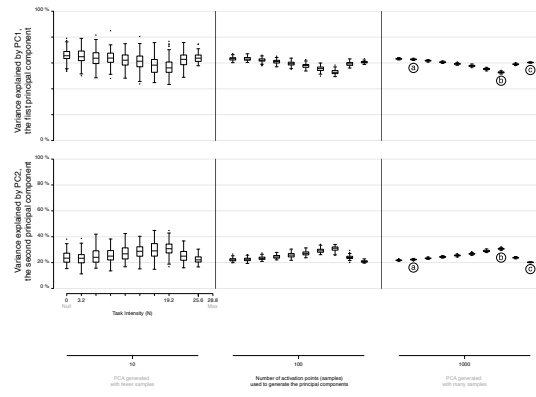
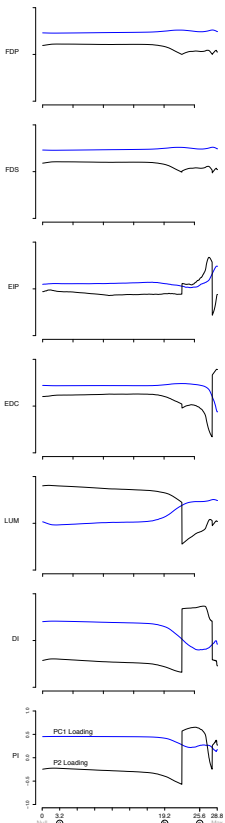


Fig. 5. Approximating the structure of feasible activation spaces via principal components analysis (PCA) is sensitive to both the number of points used and the intensity of the task. Rows show the variance explained by the first (top) and second (bottom) principal components with increasing data points (left to right). It is not possible to generalize the variance explained across tasks intensities, and large numbers of points (i.e., > 100) are needed to confidently estimate the real changes in variance explained as a function of task intensity (cf. points labeled a, b, c).

497 the PC1 and PC2 vectors change across labels a, b, and c
498 (Fig. 5) corresponding to 11, 66 and 88% of task intensity,
499 respectively. What these loadings indicate are the direction in
500 7-dimensional space, which changes dramatically.

501 These changes we see in (i) the lower and upper bounds of
502 activations, and in (ii) the relative variance explained and (iii)
503 loadings for PC1 and PC2, demonstrate that the size, shape
504 and orientation of the feasible activation space changes with
505 task intensity. Moreover, these changes represent the best-case
506 scenario given the absence of experimental noise, within- and
507 across-subject variability, and measurement error.



539 **Fig. 6. PCA loadings change dramatically as task intensity increases** For each
540 of 1,000 task intensities, we collected 1,000 points from the feasible activation space,
541 and computed three principal components. Note that the signs of the loadings depend
542 on the numerics of the PCA algorithm, and are subject to arbitrary flips in sign—
543 thus for clarity we plot them such that FDP's loadings in PC1 are positive at all
544 task intensities. Synergies at representative task intensities a, b, c in Fig. 5 differ.
545 This reflects changes in the geometric structure of the feasible activation space as
546 redundancy is lost.

547 **Changes in the probabilistic structure of the feasible activation space with increasing task intensity, or how muscle redundancy is lost.** The maximal static fingertip force vector in
548 a given direction is produced by a single and unique combination
549 of muscle activations. In contrast, any sub-maximal mag-
550 nitude of that same vector is produced by an infinite number
551 of solutions (12, 18, 19, 34). Our analysis of feasible activation
552 spaces at different task intensities allows us to characterize how
553 this redundancy changes and is lost. The histogram heatmaps
554 in Fig. 7 illustrate the changes and shrinking of within-muscle
555 density of valid activation levels for sub-maximal forces, con-

559 verging to a single solution for maximal force output. These
560 surface plots show how the normalized histograms (of 1,000
561 valid activation levels for each muscle) change at each of 100
562 levels of task intensity between 0 and 1. Following a muscle's
563 column from bottom to top shows the activation histograms
564 for each magnitude of distal force and ending, naturally, with
565 a spike about the unique value at maximal force production.

566 The flat areas in each surface plot (e.g. clearly visible
567 for DI) represent muscle activation levels that are not valid
568 for that task intensity. That is, there exist no valid muscle
569 activation patterns that contain that muscle at that level, and
570 thus no points are found there.

571 These plots show the nature and rate of convergence to the
572 unique solution for maximal force output across muscles. We
573 find that the histograms of activation levels for each muscle
574 need not be symmetric, nor have the same shape (skewness
575 and kurtosis) as the magnitude of the output force increases.
576 For some muscles the convergence accelerates after 60% or
577 80% of task intensity (as in LUM and EIP), while others
578 converge monotonically along the entire progression (e.g. DI
579 and PI). The peaks (i.e. modes) of each histogram at each
580 task intensity represents the slice of the polytope that has
581 the largest relative volume along that muscle dimension (i.e.,
582 greatest frequency of that level of muscle activation across all
583 valid solutions). Importantly, for most muscles (FDP, FDS,
584 EIP, EDC, and LUM), the mode is not necessarily located at
585 the same relative level of activation needed for maximal force
586 output. That is, the histogram at high levels of force is not
587 simply a shifted version of the histogram at low levels of force.
588 The histograms for DI are the exception, whose modes seems
589 to scale linearly with task intensity.

590 These histograms, in conjunction with the results in the
591 parallel coordinate visualization, also demonstrate that the
592 structure of feasible activation spaces cannot be inferred from
593 their bounding boxes alone (i.e., upper and lower activation
594 bounds for each muscle). An immediate example is how,
595 for most task intensities, both EIP and LUM have similar
596 lower and upper bounds near 0 and 1, respectively—yet their
597 distributions are thoroughly distinct.

Discussion

598 **Summary.** Feasibility theory, as a conceptual and computa-
599 tional approach, is a means to pierce the curse of dimensionality
600 to establish a physics-based ground truth for neuromuscular
601 control. This practical approach can now characterize—in a
602 complete way—the set of all valid ways to activate multiple
603 muscles to produce a given task. Feasible activation spaces
604 are, in fact, *the* neuromechanical landscapes upon which all
605 neuromuscular learning, control, and performance must occur.
606 Therefore, we provide an integrative and unifying perspective
607 that demonstrates how today's dominant theories of neuromuscular
608 control are alternative approximations to feasible
609 activation spaces from optimization, geometric, and proba-
610 bilistic perspectives.

611 **The value of a cost function.** Optimization is the oldest com-
612 putational approach to finding valid muscle activation patterns
613 that produce limb function (e.g., (12)). While optimization is
614 a reasonable hypotheses to explore neuromuscular control (15),
615 some criticize it as mathematical abstraction that anthropo-
616 morphizes neurons with the ability to choose, evaluate and
617 618 619 620

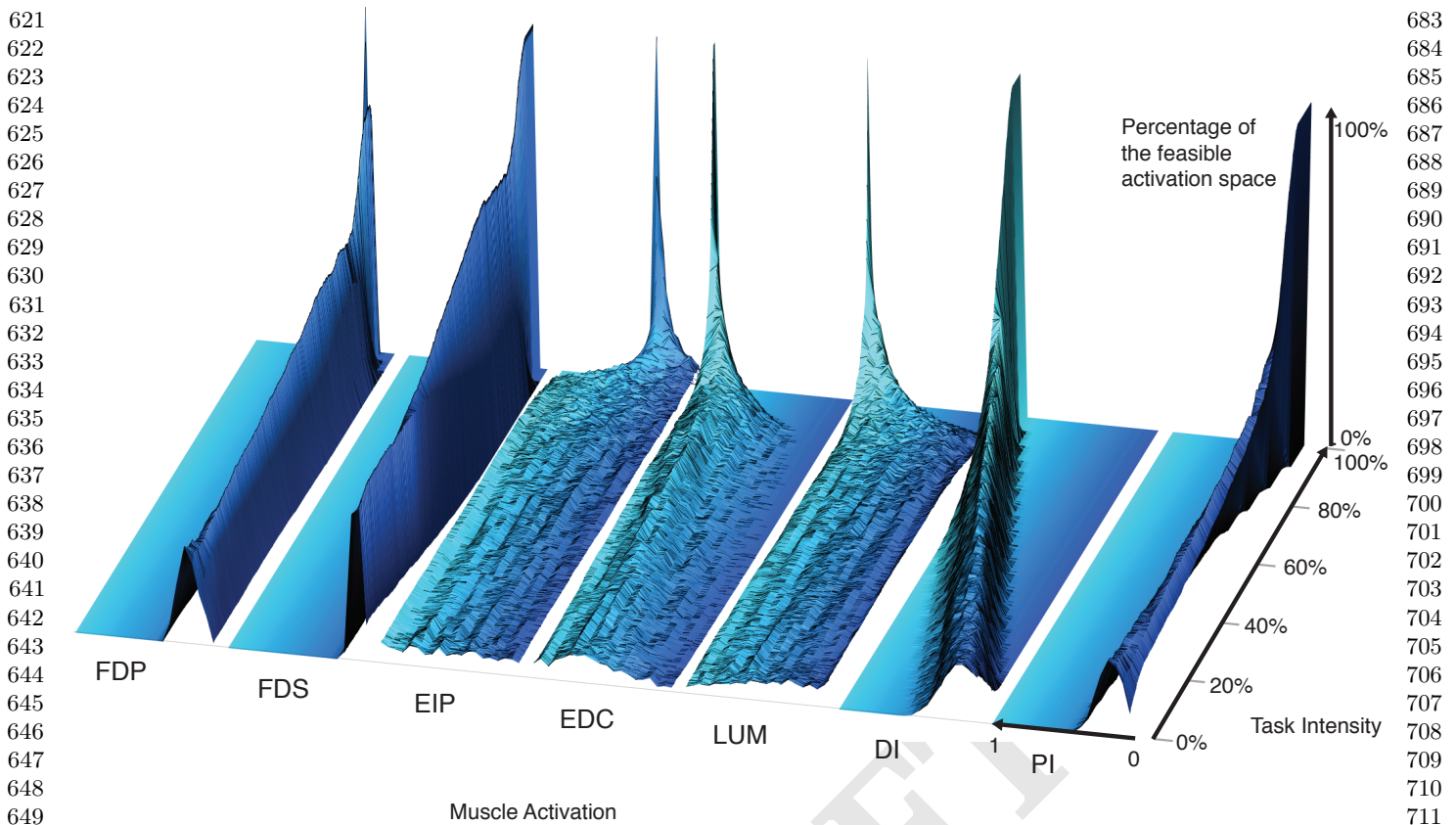


Fig. 7. The within-muscle probabilistic structure of feasible muscle patterns across 1,000 levels of fingertip task intensity. The changes in the breadth and height for each muscle reveal muscle-specific consequences of task intensity on their probability distributions. The cross-section of each density plot is the 50-bin histogram of activation for each muscle, at that task intensity. Height represents the percentage of solutions for that task. The axis going into the page indicates increasing fingertip task intensity up to 100% of maximal. Color is used to provide perspective.

follow cost functions in high-dimensions (35, 36). There is an intimate relationship between optimization and feasible activation spaces (37). Optimization is analogous to finding a best solution in the dark—guided by repeated evaluations of a cost-function. Computing the feasible activation space is then a means to ‘turn on the lights’ to see all possible valid solutions independently of cost (18). Our complete sampling of high-dimensional feasible activation spaces (38, 39) allows us to compare and contrast *families* of solutions instead of *individual* optimal solutions for a particular cost function. Fig. 3 demonstrates a complete description of families of valid coordination patterns and their relationship to alternative costs. Importantly, similar valid muscle activation patterns can have dissimilar costs, and vice versa.

Because these explorations can be done for alternative cost functions, they can provide quantitative overall descriptions of high-dimensional ‘cost landscapes.’ By not having to insist on (or settle for) individual optimal—or near-optimal—solutions, we now have the same ability the nervous system has to explore, compare and contrast multiple valid ways to coordinate muscles. Importantly, the relationships among valid muscle activation patterns emerge naturally from the physical properties of the limb and definition of the task. This cost-agnostic approach allows us to re-evaluate our assumptions about what the nervous system cares—and does not care—about. Lastly, this cost-agnostic approach also provides a powerful tool for

inverse optimization, i.e., uncovering latent cost functions from data (40). Our comparison across cost functions using parallel coordinates is already a form of inverse optimization.

Structure, correlation, and synergies. The physical properties of the limb and definition of the task also define a low-dimensional structure of the feasible activation space (18). Therefore, it is expected that experimental recordings of muscle activations during limb function will exhibit a dimensionality that is smaller than the number of muscles (1, 7). Thus, applying PCA to the points sampled from the feasible activation space also finds that few PCs can explain the variance in the data.

This application of PCA at increasing task intensities (i.e., as muscle redundancy is lost) allows us to demonstrate—for the first time to our knowledge—several important features and limitations of dimensionality reduction. For example, we see that the aspect ratio (Fig. 5) and orientation (Fig. 6) of the feasible activation spaces change as their size shrinks (Fig. 7). Thus, such *descriptive* synergies extracted from limited experimental observations likely do not generalize well across task intensities. It is important to distinguish *descriptive* synergies (the dominant approach in the literature to extract synergies from experimental data using dimensionality reduction techniques such as PCA) from *prescriptive* synergies (those known to be implemented by the controller) (18).

This also has important consequences to motor control and

745 learning. Producing force vectors at the endpoint of a finger
746 or limb with accurate magnitude and direction are critical
747 for versatile manipulation and locomotion (41–43). If a given
748 synergy can produce such accurate force vectors only for a
749 given task intensity (and thus inaccurate ones at other in-
750 tensities), then the attractiveness of synergies to simplify the
751 neuromuscular control of the limb is reduced. To compensate,
752 the nervous system would need to learn, recall and implement
753 specific synergies for each force level. In prior experimental
754 work, we have shown that the nervous system produces accu-
755 rate fingertip forces of different magnitudes by, instead, likely
756 scaling a remembered muscle activation pattern to produce
757 forces of different magnitudes, together with a full-dimensional,
758 real-time error correction neural controller (44). Note that
759 interpreting this experimental result still as a synergy-based
760 approach would defeat the purpose of synergies as a means to
761 simplify the control by reducing its dimensionality.

762 Our results also show how experiments with realistically
763 moderate numbers of participants and test trials likely do
764 not contain sufficient data to produce robust estimates of de-
765 scriptive synergies across task intensities. As per the curse
766 of dimensionality, sampling uniformly at random from high-
767 dimensional spaces is exponentially difficult. Thus, even for
768 this anatomically complete 7-muscle finger model, PCA de-
769 pends strongly on the number of independent observations,
770 such as uncorrelated trials from one subject or different sub-
771 jects. Figure 5 shows that 100 to 1,000 such ideal data points
772 from a simulated ‘test subject’ are needed to produce accurate
773 estimates of changes in PC1 and PC2 with task intensity (c.f.
774 labels a vs. b vs. c). Future studies should explore how many
775 experimental data points are sufficient from a given subject
776 when recording from only a subset of the many (20+) muscles
777 of human limbs in the presence of experimental noise, inherent
778 stochasticity of EMG, and within- and between-subject vari-
779 ability. Some studies have begun to ask subjects to explore
780 different ways to perform a given task (45) (i.e., estimate
781 the structure of the feasible activation space), but in practice
782 such studies cannot likely collect sufficient data uniformly
783 at random to obtain accurate estimates of the descriptive
784 synergies (1). While our results suggest caution when inter-
785 preting synergies obtained experimentally, we underscore that
786 dimensionality-reduction is a useful approach to capture global
787 geometric properties of feasible activation spaces.

788

789 **Toward probabilistic neuromuscular control.** Our results are
790 particularly empowering for the emerging field of probabilistic
791 neuromuscular control (8? –10). Suppose that the nervous
792 system uses some form of probabilistic or Bayesian learning
793 and control strategy. Such approach requires two enabling—
794 and biologically feasible—elements: *trial-and-error iterative*
795 *exploration*, and *memory-based exploitation* of the probability
796 density functions used to approximate the feasible activation
797 spaces (8). The parallel coordinate plots and histograms
798 in Fig. 2 and 7 provide, to our knowledge, the first com-
799 plete (38, 39) characterization of such multi-dimensional joint
800 probability density functions for a realistic tendon-driven sys-
801 tem performing a well-defined task.

802 These techniques and results now empower the study of
803 fundamental aspects of probabilistic control. For example, an
804 organism can only execute so many trial-and-error iterations
805 during learning, likely too few to completely and exhaustively
806 sample the high-dimensional feasible space of interest. This

807 makes it much more likely that, by virtue of being more
808 easily found, an organism will find and preferentially exploit
809 the strong modes (i.e., narrow and high peaks in Figs. 3, 4,
810 and 7) of the multi-dimensional probability density functions
811 than any other region of feasible activation spaces. Thus,
812 first, the maximal ranges of feasible activations described by
813 the bounding box (29, 30) may have little practical bearing
814 on how those tasks are learned and executed. And second,
815 those same strong modes would represent strong attractors
816 to create and reinforce motor habits. Habitual control has
817 been proposed based on experimental and empirical data as an
818 alternative to a strict optimization approach to neuromuscular
819 control (35). Our work now provides the computational means
820 to link habitual to probabilistic control. This allows us to
821 generate testable hypotheses of how these motor habits are
822 defined by the structure of the feasible activation space, how
823 they are learned by the organism, and how difficult or easy it
824 is to break out of them.

825 Thus, motor learning likely needs to proceed from adopting
826 easily-found solutions independently of their cost, to using
827 some low dimensional approximation to the gradient of the cost
828 landscape, to then transitioning to less likely but potentially
829 less costly subregions of the solutions space. This integrative
830 perspective leads us to propose a hybrid approach to motor
831 learning and execution where the practical limits on trial-and-
832 error iterations are coupled with the low-dimensional structure
833 of the solution space to enable some form of heuristic local
834 optimization to create sub-optimal motor habits. Importantly,
835 the organism performs strict optimization or synergy control at
836 its peril. Take, for example, the case of a 2-dimensional feasible
837 activation space embedded in 3-D, Fig. ??e. Taking a step from
838 any one valid point to another valid point on the plane runs the
839 risk of ‘falling off’ the solution space and failing at the task—a
840 risk that is exponentially exacerbated in higher-dimensions.
841 Thus, improvements in the neighborhood of a good solution
842 necessarily risk task failure and potential injury. These are all
843 arguments in support of the evolutionary and developmentally
844 useful strategy to use good-enough control based on habit or
845 sensorimotor memory rather than optimization (35, 46). This
846 may explain why mass practice and coaches are so critical to
847 achieve elite athletic performance (47).

848 **Clinical implications.** This line of thinking has consequences
849 to neurorehabilitation. Neurological conditions disrupt feasi-
850 ble activation spaces, be it by affecting anatomy of the limb,
851 muscle strength and independence with which muscles can be
852 controlled. Functional recovery following the disruption, if
853 not destruction, of the landscape of valid muscle activation
854 patterns requires re-learning existent, or building new, proba-
855 bility density functions. This occurs just when older adults
856 suffer from reduced perceptuo-motor learning rates (48).

857 A probabilistic landscape for neuromuscular function begins
858 to explain why neurorehabilitation in aging adults is so difficult
859 (e.g., (49)) and why motor learning in children takes thousands
860 of repetitions (50)—while also generating new rehabilitation
861 strategies, and testable hypotheses around them, that leverage
862 knowledge of the nature and structure of feasible activation
863 spaces.

864 **Author Affiliations.** Include department, institution, and com-
865 plete address, with the ZIP/postal code, for each author. Use
866 lower case letters to match authors with institutions, as shown
867

869	in the example. Authors with an ORCID ID may supply this	931																
870	information at submission.	932																
871		933																
872	Submitting Manuscripts. All authors must submit their arti-	934																
873	cles at PNAScentral . If you are using Overleaf to write your	935																
874	article, you can use the “Submit to PNAS” option in the top	936																
875	bar of the editor window.	937																
876		938																
877	Format. Many authors find it useful to organize their	939																
878	manuscripts with the following order of sections; Title, Author	940																
879	Affiliation, Keywords, Abstract, Significance Statement, Re-	941																
880	sults, Discussion, Materials and methods, Acknowledgments,	942																
881	and References. Other orders and headings are permitted.	943																
882		944																
883	Manuscript Length. PNAS generally uses a two-column	945																
884	format averaging 67 characters, including spaces, per line. The	946																
885	maximum length of a Direct Submission research article is six	947																
886	pages and a PNAS PLUS research article is ten pages includ-	948																
887	ing all text, spaces, and the number of characters displaced	949																
888	by figures, tables, and equations. When submitting tables,	950																
889	figures, and/or equations in addition to text, keep the text for	951																
890	your manuscript under 39,000 characters (including spaces) for	952																
891	Direct Submissions and 72,000 characters (including spaces)	953																
892	for PNAS PLUS.	954																
893		955																
894	References. References should be cited in numerical order	956																
895	as they appear in text; this will be done automatically via	957																
896	bibtex, e.g. (?) and (??). All references, including	958																
897	for the SI, should be included in the main manuscript file.	959																
898	References appearing in both sections should not be duplicated.	960																
899	SI references included in tables should be included with the	961																
900	main reference section.	962																
901		963																
902	Data Archival. PNAS must be able to archive the data essential	964																
903	to a published article. Where such archiving is not possible,	965																
904	deposition of data in public databases, such as GenBank, Ar-	966																
905	rayExpress, Protein Data Bank, Unidata, and others outlined	967																
906	in the Information for Authors, is acceptable.	968																
907		969																
908		970																
909		971																
910		972																
911		973																
912		974																
913		975																
914		976																
915		977																
916	Table 1. Comparison of the fitted potential energy surfaces and ab	978																
917	initio benchmark electronic energy calculations	979																
918		980																
919	<table border="1"><thead><tr><th>Species</th><th>CBS</th><th>CV</th><th>G3</th></tr></thead><tbody><tr><td>1. Acetaldehyde</td><td>0.0</td><td>0.0</td><td>0.0</td></tr><tr><td>2. Vinyl alcohol</td><td>9.1</td><td>9.6</td><td>13.5</td></tr><tr><td>3. Hydroxyethylidene</td><td>50.8</td><td>51.2</td><td>54.0</td></tr></tbody></table>	Species	CBS	CV	G3	1. Acetaldehyde	0.0	0.0	0.0	2. Vinyl alcohol	9.1	9.6	13.5	3. Hydroxyethylidene	50.8	51.2	54.0	981
Species	CBS	CV	G3															
1. Acetaldehyde	0.0	0.0	0.0															
2. Vinyl alcohol	9.1	9.6	13.5															
3. Hydroxyethylidene	50.8	51.2	54.0															
920		982																
921		983																
922		984																
923		985																
924	nomenclature for the TSs refers to the numbered species in the table.	986																
925		987																
926		988																
927	Supporting Information (SI). The main text of the paper must	989																
928	stand on its own without the SI. Refer to SI in the manuscript	990																
929	at an appropriate point in the text. Number supporting figures	991																
930	and tables starting with S1, S2, etc. Authors are limited to	992																
931																		
932																		
933																		
934																		
935																		
936																		
937																		
938																		
939																		
940																		
941																		
942																		
943																		
944																		
945																		
946																		
947																		
948																		
949																		
950																		
951																		
952																		
953																		
954																		
955																		
956																		
957																		
958																		
959																		
960																		
961																		
962																		
963																		
964																		
965																		
966																		
967																		
968																		
969																		
970																		
971																		
972																		
973																		
974																		
975																		
976																		
977																		
978																		
979																		
980																		
981																		
982																		
983																		
984																		
985																		
986																		
987																		
988																		
989																		
990																		
991																		
992																		

$$\begin{aligned}
 (x+y)^3 &= (x+y)(x+y)^2 \\
 &= (x+y)(x^2 + 2xy + y^2) \\
 &= x^3 + 3x^2y + 3xy^2 + y^3.
 \end{aligned}$$

[1]

no more than 10 SI files, not including movie files. Authors who place detailed materials and methods in SI must provide sufficient detail in the main text methods to enable a reader to follow the logic of the procedures and results and also must reference the online methods. If a paper is fundamentally a study of a new method or technique, then the methods must be described completely in the main text. Because PNAS edits SI and composes it into a single PDF, authors must provide the following file formats only.

SI Text. Supply Word, RTF, or LaTeX files (LaTeX files must be accompanied by a PDF with the same file name for visual reference).

Table 1. Comparison of the fitted potential energy surfaces and ab initio benchmark electronic energy calculations

Species	CBS	CV	G3
1. Acetaldehyde	0.0	0.0	0.0
2. Vinyl alcohol	9.1	9.6	13.5
3. Hydroxyethylidene	50.8	51.2	54.0

nomenclature for the TSs refers to the numbered species in the table.

Supporting Information (SI). The main text of the paper must stand on its own without the SI. Refer to SI in the manuscript at an appropriate point in the text. Number supporting figures and tables starting with S1, S2, etc. Authors are limited to

993 **SI Figures.** Provide a brief legend for each supporting figure
994 after the supporting text. Provide figure images in TIFF, EPS,
995 high-resolution PDF, JPEG, or GIF format; figures may not
996 be embedded in manuscript text. When saving TIFF files, use
997 only LZW compression; do not use JPEG compression. Do
998 not save figure numbers, legends, or author names as part of
999 the image. Composite figures must be pre-assembled.
1000

1001 **3D Figures.** Supply a composable U3D or PRC file so that it
1002 may be edited and composed. Authors may submit a PDF file
1003 but please note it will be published in raw format and will not
1004 be edited or composed.
1005

1006 **SI Tables.** Supply Word, RTF, or LaTeX files (LaTeX files must
1007 be accompanied by a PDF with the same file name for visual
1008 reference); include only one table per file. Do not use tabs or
1009 spaces to separate columns in Word tables.
1010

1011 **SI Datasets.** Supply Excel (.xls), RTF, or PDF files. This file
1012 type will be published in raw format and will not be edited or
1013 composed.
1014

1015 **SI Movies.** Supply Audio Video Interleave (avi), Quicktime
1016 (mov), Windows Media (wmv), animated GIF (gif), or MPEG
1017 files and submit a brief legend for each movie in a Word or
1018 RTF file. All movies should be submitted at the desired re-
1019 production size and length. Movies should be no more than
1020 10 MB in size.
1021

1022 **Still images.** Authors must provide a still image from each video
1023 file. Supply TIFF, EPS, high-resolution PDF, JPEG, or GIF
1024 files.
1025

1026 **Appendices.** PNAS prefers that authors submit individual
1027 source files to ensure readability. If this is not possible, supply
1028 a single PDF file that contains all of the SI associated with
1029 the paper. This file type will be published in raw format and
1030 will not be edited or composed.
1031

Materials and Methods

1032 The methods to obtain feasible activation spaces for ‘tendon-driven’
1033 limbs are described in detail in the textbook *Fundamentals of*
1034 *Neuromechanics* and references therein (18). This tendon-driven
1035 approach explicitly and distinctly avoids the conceptual approach
1036 to combine multiple muscle actions into net torques at each joint.
1037 Rather, it emphasizes studying the individual actions of all muscles
1038 at all levels of analysis, from their neural activation to their
1039 contributions to fingertip force. We describe them briefly here.
1040

1041 **Theory.** As described in (18), consider a tendon-driven limb, such as
1042 a finger, with n independently controllable muscles, where we define
1043 the neural command to each muscle as a positive value of activation
1044 between 0 (no activation) and 1 (maximal activation). We can then
1045 visualize the set of all feasible neural commands (i.e., all possible
1046 muscle activation patterns) as the points contained in a positive
1047 n -dimensional cube with sides of length equal to 1. A specific muscle
1048 activation pattern is a *point* (i.e., an n -dimensional vector \mathbf{a}) in this
1049 n -dimensional cube (12, 19–21). Now consider a specific task, such
1050 as producing a vector of static force with the fingertip, as when
1051 holding an object. Clearly, not all muscle activation patterns inside
1052 the n -dimensional cube can produce that desired static fingertip
1053 force vector: The lengths of the bones, the number and type of
1054 kinematic degrees of freedom, the anatomical routing of the tendons
the need to control individual tendons, and the physics of a motor

task uniquely specify a polytope embedded in \mathbb{R}^n (i.e., the feasible
activation space). This polytope contains the family of (potentially
infinite) valid muscle activation patterns that can produce this static
force production task. However, these valid muscle coordination
patterns are not arbitrarily different because, by construction, the
geometric structure of the polytope that contains them defines strict
spatial correlations among them (1).

System of linear equations to simulate static force production by a tendon-driven system Consider producing a vector of static force with the endpoint of the limb in a given posture. The constraints that define that task (i.e., the direction and magnitude of the force vector at the endpoint) are linear equations (18) that come from the mapping between neural activation of individual muscles to static endpoint forces and torques the limb can produce. This mapping is linearly modeled by the equation

$$\begin{pmatrix} f_x \\ f_y \\ f_z \\ \tau_x \\ \tau_y \\ \tau_z \end{pmatrix} = \mathbf{w} = H\mathbf{a} = H \begin{pmatrix} a_1 \\ a_2 \\ a_3 \\ \dots \\ a_n \end{pmatrix}, \mathbf{a} \in [0, 1]^n \quad [2]$$

where H is the matrix of linear constraints defined by the musculoskeletal anatomy of the limb (29), \mathbf{a} is the input vector of n muscle activations, $\mathbf{f} \in \mathbb{R}^m$ is the m -dimensional limb output ‘wrench’ (i.e., the forces and torques the finger can produce at the endpoint).

The output wrench, m , is at most 6-dimensional (i.e., 3 forces and 3 torques) depending on the number of kinematic degrees of freedom of the limb, and usually $m < n$ because limbs have more muscles than kinematic degrees of freedom (18). Muscles can only pull, so elements of \mathbf{a} cannot be negative, and are capped at 1 (i.e., 100% of maximal muscle activation).

What are the muscle coordination patterns that produce a given task? As explained in (18), the task of producing a static fingertip force vector is defined by specifying the desired values for the elements of the endpoint forces and torques of \mathbf{w} . Each such constraint equation defines a hyperplane of dimension $n-1$, and their combination defines the task completely. The *feasible activation space* of the task, if it is well posed (37), is defined by the points \mathbf{a} that lie within the n -cube and at the intersection of all constraint hyperplanes.

Geometrically speaking, the feasible activation space is a $(n-m)$ -dimensional convex polytope P embedded in \mathbb{R}^n that contains all n -dimensional muscle coordination patterns (i.e., points \mathbf{a}) that satisfy all constraints, and therefore can produce the task. Increasing task specificity by adding more constraints naturally decreases the dimensionality and changes the size and shape of the feasible activation space (20, 30, 51).

The Hit-and-Run algorithm uniformly samples from feasible activation spaces The goal is to characterize the qualities that define all valid muscle activation patterns (i.e., n -dimensional vectors \mathbf{a}), that are points that make up P . This is equivalent to characterizing the structure of the convex polytope P . But calculating the geometric properties of convex polytopes in high dimensions is computationally challenging. Taking the generalized concept of an n -dimensional volume as an example of a geometric property of interest, the exact volume computations for n -dimensional polytopes is known to be tractable only in a polynomial amount of time (i.e., #P-hard) (52). Currently available volume algorithms can only handle polytopes embedded in small dimensions like 10 or slightly more (53). Studying vertebrate limbs in general, however, can require including several dozen muscles, such as our studies of a 17-muscle human arm and a 31-muscle cat hindlimb model (29); and other limb models have over 40 muscles such as (1, 54–56).

Similar difficulties arise when computing other geometric properties such as the shape and aspect ratio of P in high dimensions. We and others have described polytopes P by their bounding box (i.e., the range of values in every dimension) (30, 33), but that singularly overestimates the shape and volume of the feasible activation space as discussed in (29). Take Fig. ??e as an example, where the bounding box of the 2-dimensional polygon has a volume—even though a plane has zero volume—, and can be almost as large as the positive unit cube itself. Similar problems arise in the interpretation of the inscribed and circumscribed ball (57).

We propose a complete probabilistic method to describe the structure of feasible activation spaces P . This includes the descriptive statistics, histograms, and point densities of the set of valid muscle activation patterns \mathbf{a} uniformly sampled from the polytope. To do so, we use the Hit-and-Run method. We have presented a detailed explanation of the theory (In Chapter X of (?)), have justified the utility of this method on tendon-driven models of the index finger (?).

Example of a tendon-driven system.

Realistic 3-D model of a 7-muscle human index finger We applied this methodology to our published model of an index finger for static fingertip force production. The model is described in detail elsewhere (58). Briefly, the input to the model is a 7-D muscle activation pattern \mathbf{a} , and the output is a 4-D wrench (i.e., static forces and torque) at the fingertip \mathbf{w}

$$\mathbf{w} = H\mathbf{a}$$

$$H = J^{-T}RF_o$$

$$H \in \mathbb{R}^{4 \times 7}$$

where

$$\mathbf{a} = \begin{pmatrix} a_{FDP} \\ a_{FDS} \\ a_{EIP} \\ a_{EDC} \\ a_{LUM} \\ a_{DI} \\ a_{PI} \end{pmatrix} \quad [6]$$

In Cartesian coordinates, the 4-dimensional output wrench corresponds to the anatomical directions shown in Fig. 1e.

$$\mathbf{w} = \begin{pmatrix} f_x \\ f_y \\ f_z \\ \tau_x \end{pmatrix} = \begin{pmatrix} f_{radial} \\ f_{distal} \\ f_{palmar} \\ \tau_{radial} \end{pmatrix} \quad [7]$$

The biomechanical model H includes three serial links articulated by four kinematic degrees of freedom (ad-abduction, flexion-extension at the metacarpophalangeal joint, and flexion-extension at the proximal and distal interphalangeal joints). The action of each of the seven muscles (FDP: *flexor digitorum profundus*, FDS: *flexor digitorum superficialis*, EIP: *extensor indicis proprius*, EDC: *extensor digitorum communis*, LUM: *lumbrical*, DI: *dorsal interosseous*, and PI: *palmar interosseous*) on each joint to produce torque is given by the moment arm matrix $R \in \mathbb{R}^{4 \times 4}$. Lastly, $J \in \mathbb{R}^{4 \times 4}$ and $F_o \in \mathbb{R}^{7 \times 7}$ are the Jacobian of the fingertip with 4 kinematic degrees of freedom, and the diagonal matrix containing the maximal strengths of the seven muscles, respectively (18, 44). The finger posture was defined to be 0° ad-abduction and 45° flexion at the metacarpophalangeal joint, and 45° and 10° flexion, respectively, at the proximal and distal interphalangeal joints.

Feasible activation space for a static fingertip force task Our goal is to find the family of all feasible muscle activation patterns that can produce a given task. In particular, the task we explored is producing various magnitudes of a submaximal static force in the distal direction f_{distal} — in the absence of any τ_{radial} , shown in Fig. 1f. Therefore the feasible activation space is a polytope P in 7-dimensional activation space that meets the following four linear constraints in \mathbf{a} (18, 21, 44)

$$f_{radial} = 0 \quad [8]$$

$$f_{distal} = \text{desired magnitude as \% of maximal} \quad [9]$$

$$f_{palmar} = 0 \quad [10]$$

$$\tau_{palmar} = 0 \quad [11]$$

These four constraints on the static output of the finger yield a 3-dimensional (i.e., $7 - 4 = 3$) polytope P embedded in 7-dimensional activation space. For details on how to create such models, apply task constraints and find such polytopes via vertex enumeration methods, see (18).

Thus all valid output wrenches will have the form

$$\mathbf{w} = \begin{pmatrix} 0 \\ \text{Desired distal task intensity in N} \\ 0 \\ 0 \end{pmatrix} \quad [12]$$

For the index finger model used in this paper, the published maximal feasible force in the distal direction is 28.81 Newtons. We defined the normalized desired distal task intensity as a value ranging between 0 and 1, i.e., each submaximal force can be produced by any of the points contained in its corresponding feasible activation space. For the production of a maximal force with $\alpha = 1$ the feasible activation space shrinks to a single point (12, 19, 37, 44).

Analysis of feasible activation spaces.

Parallel coordinates visualization shows the location of all points across all dimensions

Parallel coordinates are a common graphical approach to visualize interactions among high-dimensional data, which has been used in biomechanical studies (59, 60). To demonstrate this visualization method, consider the results of the simple 3-dimensional example shown in Fig. ???. We begin by drawing n parallel vertical lines for each of the dimensions n (i.e., 3 muscles). With the axis limits of each line set between 0 and 1, each point (Fig. 2a) is then represented by connecting their coordinates by $n - 1$ lines as shown in Fig. 2b.

Neural and metabolic cost functions As mentioned in the Introduction, the field of neuromuscular control has a long historical tradition of using optimization to find muscle activation patterns that minimize effort, which requires the (often contentious) definition of cost functions (12, 13, 16, 19). Therefore, we used four representative cost functions to calculate the relative fitness of each of the muscle activation patterns sampled—in effect also calculating the fitness landscape across all possible solutions. The cost functions are defined at the level of neural effort (L_1 , and L_2 norms); and at the level of metabolic cost, thought to be approximated by neural drive weighted by the strength of each muscle (L_1^w and L_2^w norms) (13, 16).

To visualize the costs associated with each valid muscle coordination pattern, we simply added four vertical lines at the far right of the parallel coordinates plot, one for each cost function, Fig. 2c. The variables a_i and F_{0i} represent the activation of the i^{th} muscle in a given muscle activation pattern, and the maximal strength of each muscle (13, 16). Maximal muscle strengths are approximated by multiplying each muscle's physiological cross-sectional area, in cm^2 , by the maximal active muscle stress of mammalian muscle, 35 N/cm^2 (61). These four cost functions are but four examples as the literature contains many others as any investigator is in fact free to chose any cost function deemed relevant to their study.

Histograms of the activation level of each muscle across all valid solutions Muscle-by-muscle histograms are another straightforward way to visualize the many points sampled from the convex polytope. Histograms are particularly helpful because they are approximations to probability density functions. They visualize the relative number of solutions (i.e., density of solutions) that required a particular level of activation from a particular muscle within its range of [0, 1]. In addition, the upper and lower bounds of the histograms show, in fact, the size of the side of the bounding box of the polytope in every dimension (i.e., for independently controlled muscle).

Dimensionality reduction Investigators have repeatedly reported that electromyographical signals (i.e., experimental estimates of muscle activation patterns) tend to exhibit strong correlations with one another. In these experimental descriptions of dimensionality reduction of neuromuscular control, only few independent functions—sometimes called synergies—suffice to explain the majority of the variability in the observed muscle activation patterns (1–4, 6, 7, 62). Principal components analysis (PCA) is a widely used technique to extract these few independent basis functions (correlation vectors called principal components, PCs) from high-dimensional data (63). In this case, PCs are often called the experimental representations of synergies of neural origin (1).

Therefore, we also applied PCA to points (i.e., muscle coordination patterns) sampled from the feasible activation space at each

1241 force level. This provides the PCs that describe the correlations
 1242 among valid muscle activation patterns for a given task. For example,
 1243 the feasible activation space P in Fig. ??e is a 2-dimensional polygon embedded in 3-dimensional activation space. Thus, applying
 1244 PCA to points sampled from the polygon will extract 2 synergies (i.e., 3-dimensional correlation vectors PC1 and PC2) that wholly
 1245 explain the feasible activation space. By extension, in the case of
 1246 fingertip force production in Fig. 1, the feasible activation space is a
 1247 3-dimensional polytope embedded of the 7-dimensional activation
 1248 space. And PCA should extract, by construction, as many synergies
 1249 as there are dimensions in the feasible activation space. For static
 1250 force production with the index fingertip (i.e., 7 muscles and 4
 1251 constraints), we know that 3 principal components should describe
 1252 100% of the variance in points sampled from the feasible activation
 1253 space (i.e., 7-dimensional correlation vectors PC1, PC2, and PC3).

1254 Applying PCA to our data allows us to test whether and how
 1255 its results change when applied to feasible activation spaces for
 1256 different magnitudes of fingertip force. We applied PCA to feasible
 1257 activation spaces for fingertip task intensities ranging from 0 to 90%
 1258 of maximal. We compare both the variance explained by each PC
 1259

- 1260 1. Kutch J, Valero-Cuevas F (2012) Challenges and new approaches to proving the existence
 of muscle synergies of neural origin. *PLoS Computational Biology* 8(5):e1002434.
- 1261 2. Steele KM, Tresch MC, Perreault EJ (2013) The number and choice of muscles impact the
 results of muscle synergy analyses. *Frontiers in computational neuroscience* 7.
- 1262 3. Bizzelli E, Cheung VC (2013) The neural origin of muscle synergies. *Frontiers in computational
 neuroscience* 7.
- 1263 4. Dingwell JB, John J, Cusumano JP (2010) Do humans optimally exploit redundancy to control
 step variability in walking? *PLoS computational biology* 6(7):e1000856.
- 1264 5. Rácz K, Valero-Cuevas FJ (2013) Spatio-temporal analysis reveals active control of both
 task-relevant and task-irrelevant variables. *Frontiers in computational neuroscience* 7.
- 1265 6. Steele KM, Tresch MC, Perreault EJ (2015) Consequences of biomechanically constrained
 tasks in the design and interpretation of synergy analyses. *Journal of neurophysiology*
 113(7):2102–2113.
- 1266 7. Alessandro C, Delis I, Nori F, Panzeri S, Berret B (2013) Muscle synergies in neuroscience
 and robotics: from input-space to task-space perspectives. *Frontiers in computational neuro-
 science* 7.
- 1267 8. Kording KP, Wolpert DM (2004) Bayesian integration in sensorimotor learning. *Nature*
 427(6971):244–247.
- 1268 9. Kording KP (2014) Bayesian statistics: relevant for the brain? *Current Opinion in Neurobiol-*
 ogy 25:130 – 133. Theoretical and computational neuroscience.
- 1269 10. Bernikow M, O'Brien MK, Kording KP, Ahmed AA (2013) An examination of the generalizability
 of motor costs. *PLoS one* 8(1):e53759.
- 1270 11. Sanger TD (2011) Distributed control of uncertain systems using superpositions of linear
 operators. *Neural computation* 23(8):1911–1934.
- 1271 12. Chao E, An K (1978) Graphical interpretation of the solution to the redundant problem in
 biomechanics. *Journal of Biomechanical Engineering* 100:159–67.
- 1272 13. Puriat斯基 BI (2000) Muscle coordination: the discussion continues. *Motor Control* 4(1):97–116.
 0 1087–1640 Journal article.
- 1273 14. Scott SH (2004) Optimal feedback control and the neural basis of volitional motor control.
 Nature Reviews Neuroscience 5(7):532–546.
- 1274 15. Todorov E, Jordan MI (2002) Optimal feedback control as a theory of motor coordination.
 Nature neuroscience 5(11):1226–1235.
- 1275 16. Crowninshield R, Brand R (1981) A physiologically based criterion of muscle force prediction
 in locomotion. *Journal of Biomechanics* 14(11):793–801.
- 1276 17. Higginson J, Neptune R, Anderson F (2005) Simulated parallel annealing within a neighbor-
 hood for optimization of biomechanical systems. *Journal of biomechanics* 38(9):1938–1942.
- 1277 18. Valero-Cuevas FJ (2015) *Fundamentals of Neuromechanics, Biosystems and Biorobotics*.
 (SpringerVerlag London) Vol. 8.
- 1278 19. Spoor C (1983) Balancing a force on the fingertip of a two-dimensional finger model without
 intrinsic muscles. *Journal of Biomechanics* 16(7):497–504.
- 1279 20. Kuo A, Zajac F (1993) Human standing posture: multi-joint movement strategies based on
 biomechanical constraints. *Progress in Brain Research* 97:349–358.
- 1280 21. Valero-Cuevas FJ, Zajac FE, Burgar CG (1998) Large index-fingertip forces are produced by
 subject-independent patterns of muscle excitation. *Journal of Biomechanics* 31:693–703.
- 1281 22. Gallego JA, Perich MG, Miller LE, Solla SA (2017) Neural manifolds for the control of move-
 ment. *Neuron* 94(5):978–984.
- 1282 23. Bellman R, Osborn H (1958) Dynamic programming and the variation of green's functions.
 Journal of Mathematics and Mechanics pp. 81–85.
- 1283 24. Bellman RE (2015) *Adaptive control processes: a guided tour*. (Princeton university press).
- 1284 25. Avis D, Fukuda K (1992) A pivoting algorithm for convex hulls and vertex enumeration of
 arrangements and polyhedra. *Discrete & Computational Geometry* 8(3):295–313.
- 1285 26. Valero-Cuevas FJ, Hoffmann H, Kurse MU, Kutch JJ, Theodorou EA (2009) Computational
 models for neuromuscular function. *IEEE Reviews in Biomedical Engineering* (2) October p.
 110–135.
- 1286 27. Theodorou E, Valero-Cuevas FJ (2010) Optimality in neuromuscular systems in *Engineering
 in Medicine and Biology Society (EMBC), 2010 Annual International Conference of the IEEE*.
 (IEEE), pp. 4510–4516.
- 1287 28. Scholz JP, Schöner G (1999) The uncontrolled manifold concept: identifying control variables
 for a functional task. *Exp Brain Res* 126:289–306.
- 1288 29. Valero-Cuevas FJ, Cohn BA, Yingvason HF, Lawrence EL (2015 In Press) Exploring the high-
 dimensional structure of muscle redundancy via subject-specific and generic musculoskeletal
 models. *Journal of Biomechanics* doi:10.1016/j.biomech.2015.04.026.
- 1289 30. Sohn MH, McKay JL, Ting LH (2013) Defining feasible bounds on muscle activation in a
 redundant biomechanical task: practical implications of redundancy. *Journal of biomechanics*
 46(7):1363–1368.
- 1290 31. Venkadesan M, Valero-Cuevas FJ (2008) Neural control of motion-to-force transitions with
 their vector direction (i.e., the ‘loadings’ or correlations among
 muscle (64)) as the force level increases. Lastly, we tested whether
 our PCA results are sensitive to the number of points sampled
 from each feasible activation space. This is important because
 experimental studies test 10 or so subjects in practice, which may
 be too few when sampling from high-dimensional spaces.

1303
 1304
 1305
 1306
 1307
 1308
 1309
 1310
 1311
 1312
 1313
 1314
 1315
 1316
 1317
 1318
 1319
 1320
 1321
 1322
 1323
 1324
 1325
 1326
 1327
 1328
 1329
 1330
 1331
 1332
 1333
 1334
 1335
 1336
 1337
 1338
 1339
 1340
 1341
 1342
 1343
 1344
 1345
 1346
 1347
 1348
 1349
 1350
 1351
 1352
 1353
 1354
 1355
 1356
 1357
 1358
 1359
 1360
 1361
 1362
 1363
 1364

1303
 1304
 1305
 1306
 1307
 1308
 1309
 1310
 1311
 1312
 1313
 1314
 1315
 1316
 1317
 1318
 1319
 1320
 1321
 1322
 1323
 1324
 1325
 1326
 1327
 1328
 1329
 1330
 1331
 1332
 1333
 1334
 1335
 1336
 1337
 1338
 1339
 1340
 1341
 1342
 1343
 1344
 1345
 1346
 1347
 1348
 1349
 1350
 1351
 1352
 1353
 1354
 1355
 1356
 1357
 1358
 1359
 1360
 1361
 1362
 1363
 1364

1303
 1304
 1305
 1306
 1307
 1308
 1309
 1310
 1311
 1312
 1313
 1314
 1315
 1316
 1317
 1318
 1319
 1320
 1321
 1322
 1323
 1324
 1325
 1326
 1327
 1328
 1329
 1330
 1331
 1332
 1333
 1334
 1335
 1336
 1337
 1338
 1339
 1340
 1341
 1342
 1343
 1344
 1345
 1346
 1347
 1348
 1349
 1350
 1351
 1352
 1353
 1354
 1355
 1356
 1357
 1358
 1359
 1360
 1361
 1362
 1363
 1364

- 1303
 1304
 1305
 1306
 1307
 1308
 1309
 1310
 1311
 1312
 1313
 1314
 1315
 1316
 1317
 1318
 1319
 1320
 1321
 1322
 1323
 1324
 1325
 1326
 1327
 1328
 1329
 1330
 1331
 1332
 1333
 1334
 1335
 1336
 1337
 1338
 1339
 1340
 1341
 1342
 1343
 1344
 1345
 1346
 1347
 1348
 1349
 1350
 1351
 1352
 1353
 1354
 1355
 1356
 1357
 1358
 1359
 1360
 1361
 1362
 1363
 1364
- 1303
 1304
 1305
 1306
 1307
 1308
 1309
 1310
 1311
 1312
 1313
 1314
 1315
 1316
 1317
 1318
 1319
 1320
 1321
 1322
 1323
 1324
 1325
 1326
 1327
 1328
 1329
 1330
 1331
 1332
 1333
 1334
 1335
 1336
 1337
 1338
 1339
 1340
 1341
 1342
 1343
 1344
 1345
 1346
 1347
 1348
 1349
 1350
 1351
 1352
 1353
 1354
 1355
 1356
 1357
 1358
 1359
 1360
 1361
 1362
 1363
 1364
- 1303
 1304
 1305
 1306
 1307
 1308
 1309
 1310
 1311
 1312
 1313
 1314
 1315
 1316
 1317
 1318
 1319
 1320
 1321
 1322
 1323
 1324
 1325
 1326
 1327
 1328
 1329
 1330
 1331
 1332
 1333
 1334
 1335
 1336
 1337
 1338
 1339
 1340
 1341
 1342
 1343
 1344
 1345
 1346
 1347
 1348
 1349
 1350
 1351
 1352
 1353
 1354
 1355
 1356
 1357
 1358
 1359
 1360
 1361
 1362
 1363
 1364
- 1303
 1304
 1305
 1306
 1307
 1308
 1309
 1310
 1311
 1312
 1313
 1314
 1315
 1316
 1317
 1318
 1319
 1320
 1321
 1322
 1323
 1324
 1325
 1326
 1327
 1328
 1329
 1330
 1331
 1332
 1333
 1334
 1335
 1336
 1337
 1338
 1339
 1340
 1341
 1342
 1343
 1344
 1345
 1346
 1347
 1348
 1349
 1350
 1351
 1352
 1353
 1354
 1355
 1356
 1357
 1358
 1359
 1360
 1361
 1362
 1363
 1364
- 1303
 1304
 1305
 1306
 1307
 1308
 1309
 1310
 1311
 1312
 1313
 1314
 1315
 1316
 1317
 1318
 1319
 1320
 1321
 1322
 1323
 1324
 1325
 1326
 1327
 1328
 1329
 1330
 1331
 1332
 1333
 1334
 1335
 1336
 1337
 1338
 1339
 1340
 1341
 1342
 1343
 1344
 1345
 1346
 1347
 1348
 1349
 1350
 1351
 1352
 1353
 1354
 1355
 1356
 1357
 1358
 1359
 1360
 1361
 1362
 1363
 1364
- 1303
 1304
 1305
 1306
 1307
 1308
 1309
 1310
 1311
 1312
 1313
 1314
 1315
 1316
 1317
 1318
 1319
 1320
 1321
 1322
 1323
 1324
 1325
 1326
 1327
 1328
 1329
 1330
 1331
 1332
 1333
 1334
 1335
 1336
 1337
 1338
 1339
 1340
 1341
 1342
 1343
 1344
 1345
 1346
 1347
 1348
 1349
 1350
 1351
 1352
 1353
 1354
 1355
 1356
 1357
 1358
 1359
 1360
 1361
 1362
 1363
 1364
- 1303
 1304
 1305
 1306
 1307
 1308
 1309
 1310
 1311
 1312
 1313
 1314
 1315
 1316
 1317
 1318
 1319
 1320
 1321
 1322
 1323
 1324
 1325
 1326
 1327
 1328
 1329
 1330
 1331
 1332
 1333
 1334
 1335
 1336
 1337
 1338
 1339
 1340
 1341
 1342
 1343
 1344
 1345
 1346
 1347
 1348
 1349
 1350
 1351
 1352
 1353
 1354
 1355
 1356
 1357
 1358
 1359
 1360
 1361
 1362
 1363
 1364
- 1303
 1304
 1305
 1306
 1307
 1308
 1309
 1310
 1311
 1312
 1313
 1314
 1315
 1316
 1317
 1318
 1319
 1320
 1321
 1322
 1323
 1324
 1325
 1326
 1327
 1328
 1329
 1330
 1331
 1332
 1333
 1334
 1335
 1336
 1337
 1338
 1339
 1340
 1341
 1342
 1343
 1344
 1345
 1346
 1347
 1348
 1349
 1350
 1351
 1352
 1353
 1354
 1355
 1356
 1357
 1358
 1359
 1360
 1361
 1362
 1363
 1364
- 1303
 1304
 1305
 1306
 1307
 1308
 1309
 1310
 1311
 1312
 1313
 1314
 1315
 1316
 1317
 1318
 1319
 1320
 1321
 1322
 1323
 1324
 1325
 1326
 1327
 1328
 1329
 1330
 1331
 1332
 1333
 1334
 1335
 1336
 1337
 1338
 1339
 1340
 1341
 1342
 1343
 1344
 1345
 1346
 1347
 1348
 1349
 1350
 1351
 1352
 1353
 1354
 1355
 1356
 1357
 1358
 1359
 1360
 1361
 1362
 1363
 1364
- 1303
 1304
 1305
 1306
 1307
 1308
 1309
 1310
 1311
 1312
 1313
 1314
 1315
 1316
 1317
 1318
 1319
 1320
 1321
 1322
 1323
 1324
 1325
 1326
 1327
 1328
 1329
 1330
 1331
 1332
 1333
 1334
 1335
 1336
 1337
 1338
 1339
 1340
 1341
 1342
 1343
 1344
 1345
 1346
 1347
 1348
 1349
 1350
 1351
 1352
 1353
 1354
 1355
 1356
 1357
 1358
 1359
 1360
 1361
 1362
 1363
 1364
- 1303
 1304
 1305
 1306
 1307
 1308
 1309
 1310
 1311
 1312
 1313
 1314
 1315
 1316
 1317
 1318
 1319
 1320
 1321
 1322
 1323
 1324
 1325
 1326
 1327
 1328
 1329
 1330
 1331
 1332
 1333
 1334
 1335
 1336
 1337
 1338
 1339
 1340
 1341
 1342
 1343
 1344
 1345
 1346
 1347
 1348
 1349
 1350
 1351
 1352
 1353
 1354
 1355
 1356
 1357
 1358
 1359
 1360
 1361
 1362
 1363
 1364
- 1303
 1304
 1305
 1306
 1307
 1308
 1309
 1310
 1311
 1312
 1313
 1314
 1315
 1316
 1317
 1318
 1319
 1320
 1321
 1322
 1323
 1324
 1325
 1326
 1327
 1328
 1329
 1330
 1331
 1332
 1333
 1334
 1335
 1336
 1337
 1338
 1339
 1340
 1341
 1342
 1343
 1344
 1345
 1346
 1347
 1348
 1349
 1350
 1351
 1352
 1353
 1354
 1355
 1356
 1357
 1358
 1359
 1360
 1361
 1362
 1363
 1364
- 1303
 1304
 1305
 1306
 1307
 1308
 1309
 1310
 1311
 1312
 1313
 1314
 1315
 1316
 1317
 1318
 1319
 1320
 1321
 1322
 1323
 1324
 1325
 1326
 1327
 1328
 1329
 1330
 1331
 1332
 1333
 1334
 1335
 1336
 1337
 1338
 1339
 1340
 1341
 1342
 1343
 1344
 1345
 1346
 1347
 1348
 1349
 1350
 1351
 1352
 1353
 1354
 1355
 1356
 1357
 1358
 1359
 1360
 1361
 1362
 1363
 1364
- 1303
 1304
 1305
 1306
 1307
 1308
 1309
 1310
 1311
 1312
 1313
 1314
 1315
 1316
 1317
 1318
 1319
 1320
 1321
 1322
 1323
 1324
 1325
 1326
 1327
 1328
 1329
 1330
 1331
 1332
 1333
 1334
 1335
 1336
 1337
 1338
 1339
 1340
 1341
 1342
 1343
 1344
 1345
 1346
 1347
 1348
 1349
 1350
 1351
 1352
 1353
 1354
 1355
 1356
 1357
 1358
 1359
 1360
 1361
 1362
 1363
 1364
- 1303<br